



Short communication

One-pot synthesis of PtNi alloy nanoflowers supported on multi-walled carbon nanotubes with superior electrocatalytic activity for the oxygen reduction



Dao-Jun Guo <sup>a,\*</sup>, Shu-Kun Cui <sup>b</sup>, Dan Cheng <sup>a</sup>, Peng Zhang <sup>a</sup>, Li Jiang <sup>a</sup>, Can-Can Zhang <sup>a</sup>

<sup>a</sup> The Key Laboratory of Life-Organic Analysis, School of Chemistry and Chemical Engineering, Qufu Normal University, Qufu, Shandong 273165, PR China

<sup>b</sup> College of Elementary Education, Jining University, Qufu, Shandong 273155, PR China

HIGHLIGHTS

- Easy preparation of PtNi alloy nanoflower catalyst by one-pot reaction.
- PtNi alloys exhibit superior structure stability compared with Pt/C (JM).
- Enhanced catalytic activity for the ORR of the nanocatalyst in acid media.

ARTICLE INFO

Article history:

Received 28 September 2013

Received in revised form

29 December 2013

Accepted 30 December 2013

Available online 8 January 2014

Keywords:

Platinum–nickel alloy

Nanoflowers

Oxygen reduction

Electrocatalysts

Fuel cell

ABSTRACT

Well-defined PtNi alloy nanoflowers supported on multi-walled carbon nanotubes (PtNi-H/MWCNTs) are successfully synthesized through a novel and potentially general one-pot reaction that exploits an in situ sacrificial template. The detailed morphology, composition, and structure of the PtNi alloy nanoflowers are investigated by transmission electron microscopy, energy-dispersive X-ray spectroscopy, nitrogen adsorption–desorption isotherms and X-ray diffraction. The results demonstrate that the PtNi-H/MWCNTs are highly porous. The electrocatalytic activity and stability of the PtNi-H/MWCNTs for the oxygen reduction reaction (ORR) are investigated by rotating disk electrode voltammetry in 0.1 mol L<sup>-1</sup> HClO<sub>4</sub> solution. The electrochemical tests indicated that PtNi-H/MWCNTs exhibited superior ORR activity along with satisfactory stability and methanol-tolerance under acidic conditions, which made them promising electrocatalysts.

© 2014 Elsevier B.V. All rights reserved.

## 1. Introduction

The promise of direct conversion of chemical energy into electrical energy makes fuel cell development an area of technological interest owing to their high efficiency, high power density and low pollution emission. In recent years, many groups of researchers are working intensively in the development of novel electrocatalysts and membranes for polymer electrolyte fuel cells (PEMFC) with the goal of attaining practical power density levels and reducing costs in the mobile and portable devices [1]. But in PEMFC, the slow rate of oxygen reduction reaction (ORR) causes a large over-potential at low temperatures [2,3]. Therefore, development of highly active cathode electrocatalysts is essential. Better electrocatalytic properties of Pt-alloys as well other noble metals-alloys than of Pt, have

been related to different phenomena broadly classified as: i) structural, ii) electronic and iii) surface sensitive factors [4,5]. For example, different studies have revealed that modifying the M<sub>1</sub>–M<sub>2</sub> distance through lattice contraction or expansion due to alloying effect, may decrease the OH adsorption energy on Pt-alloy increasing ORR activity [6,7]. Alloying Pt with metals such as cobalt (Co), iron (Fe) and nickel (Ni) is an efficient route to enhance the catalytic activity for the ORR due to the formation of a new electronic structure. [8–14] The concept of alloying to enhance the activity of ORR has been implemented both in case of PEMFCs [8–10,15] and direct methanol fuel cells [16–20].

Among the numerous investigations concerning the synthesis of new electrocatalysts for enhancing both the electrocatalytic activity and durability regarding the ORR in PEM fuel cells, the porous nanostructures with nanopores have attracted considerable attention particularly in the field of fuel cells. Such porous nanostructures have high surface area to volume ratios and low density, so they can supply enough active sites for oxygen reduction

\* Corresponding author. Tel.: +86 537 4453161.

E-mail address: [guodaojun03@163.com](mailto:guodaojun03@163.com) (D.-J. Guo).

reaction [21,22]. Meanwhile, the particular nanoporosity is in favor of O<sub>2</sub> mass transport through the metal surface, thus enhancing the ORR kinetic process [23].

Despite the above observations still work is needed to improve the catalytic activity of the PtNi catalyst system and to gain further insight into catalyst structure. In the literature, little work has been devoted to carbon nanotube-supported PtNi alloy nanoflower catalysts for methanol oxidation in acid media. We report in this paper on the preparation of PtNi alloy nanoflowers supported on MWCNTs with atomic ratio of Pt to Ni of 1:1 by a novel and potentially general one-pot reaction that exploits an *in situ* sacrificial template. The prepared PtNi alloy nanoflower catalysts have been characterized with physical techniques to elucidate their structural features, while their electrochemical properties have been studied with CV and CO stripping to evaluate their electrocatalytic activity toward oxygen electro-reduction reaction in acid media. The as-prepared PtNi alloy nanoflower electrocatalyst shows relatively high catalytic activity towards the reduction of oxygen.

## 2. Experimental

### 2.1. Synthesis of PtNi-H/MWCNT nanoflowers

In a typical synthesis, carbon nanotubes (48 mg) were pre-treated with 5 M HCl and concentrated HNO<sub>3</sub> solution before being suspended in 20 mL of deionized water. NiCl<sub>2</sub>·6H<sub>2</sub>O (11.3 mg) and poly(vinyl pyrrolidone) (PVP, MW = 40 000, 130 mg) are dissolved in 100 mL of NANOpure H<sub>2</sub>O (18.2 MΩ), sonicated for 30 min, and purged with Ar for 30 min. MWCNT supports were then added to the above solution, sonicated for 15 min. A freshly prepared solution of NaBH<sub>4</sub> (15 mg in 40 mL of H<sub>2</sub>O) is then added dropwise under stirring. Immediately after all of the NaBH<sub>4</sub> has been added, K<sub>2</sub>PtCl<sub>6</sub> (23.1 mg in 40 mL H<sub>2</sub>O) (atomic ratio of Pt and Ni = 1:1) is added dropwise with stirring. After 30 min, the product is collected by centrifugation, washed several times with H<sub>2</sub>O and ethanol, the obtained catalyst was dried in a vacuum oven at 70 °C overnight, the PtNi-H/MWCNT (20%wt PtNi) nanoflowers were obtained. The ORR activities of the commercial Johnson-Matthey Pt/C (20 wt% Pt on carbon) (Pt/C-JM) catalysts were also measured for comparison.

### 2.2. Measurements

Cyclic voltammetry (CV) experiments to measure the charge associated with hydrogen adsorption were conducted in an argon saturated 0.1 mol L<sup>-1</sup> perchloric acid (HClO<sub>4</sub>) electrolyte at a scan rate of 50 mV s<sup>-1</sup> using a three-electrode cell with the PARSTAT 2273 potentiostat controlled by PowerSuite® software (Princeton Applied Research). The oxygen reduction reaction (ORR) measurement was performed on a PAR model 636 rotating disk electrode (RDE) system in an O<sub>2</sub>-saturated 0.1 mol L<sup>-1</sup> HClO<sub>4</sub> solution. The catalyst suspension solution was prepared by sonicating 0.5 mg of sample and 1 mL ethanol. Then 10 μL of as prepared catalyst suspension and 3 μL 0.05% nafion were dropped onto a 4 mm-diameter glassy carbon (GC) electrode, which was pre-polished to a mirror-finish with 0.05 μm alumina slurry and used as the working electrode. Pt gauze and a freshly prepared reversible hydrogen electrode (RHE) were used as counter electrode and reference electrode, respectively. All potentials in this report are quoted versus RHE.

The morphology of PtNi-H/MWCNT nanoflowers were investigated using transmission electron microscopy (TEM, JEOL model JEM-2011) operated at 200 keV and equipped with an energy-dispersive spectrometer (EDS). The X-ray diffraction (XRD) analysis was performed using the Bruker D8 advanced X-ray

diffractometer with Cu Kα radiation ( $\lambda = 1.5418 \text{ \AA}$ ). Nitrogen adsorption-desorption isotherms (SADI) experiments were performed at 77 K on Micromeritics ASAP 2020 MC instrument to determine the Brunauer–Emmett–Teller (BET) surface area and pore size distribution.

## 3. Results and discussion

### 3.1. TEM analysis and elemental composition of PtNi-H/MWCNT nanoflowers

The structural features of the as-prepared PtNi-H/MWCNT nanoflowers were first investigated by TEM. The low resolution TEM images of Fig. 1A reveal that the as-synthesized products are flower-like structures with average particle diameters of 25–100 nm. Further detailed observation shows that each of the nanoflowers is actually a three-dimensionally interconnected porous nanostructure and seems to be assembled from many smaller grains with 4–7 nm diameter, rather than discrete individual nanoparticle (Fig. 1B). The compositions of the PtNi-H/MWCNT nanoflowers were investigated by EDS. According to EDS data, the atomic ratio of Pt and Ni in the PtNi-H/MWCNT nanoflowers is ca. 1:1 (Fig. 1C), in accordance with the theoretical stoichiometric proportion. The resulting patterns show that the formation of PtNi alloy nanoflowers, which is a significant result, is directly related to the synthetic details involved in the one-pot reaction. There is excess BH<sub>4</sub><sup>-</sup> in the reaction flask, so any Ni that is oxidized to Ni<sup>2+</sup> during Pt deposition will be reduced back to Ni. At the same time, PVP is present as the surface stabilizer, and its long polymeric chain structure will completely surround one or more nanospheres. Since PVP is known to bind metal cations [24,25], it can trap the Ni<sup>2+</sup> that is liberated during the galvanic displacement reaction and allow it to combine with Pt<sup>4+</sup> and be co-reduced near the surface of the template nanosphere. The result is a shell that contains both Ni and Pt in the form of an alloy [26].

### 3.2. N<sub>2</sub> sorption and XRD analysis of PtNi-H/MWCNT nanoflowers

To further confirm the porous structure of the PtNi-H/MWCNT nanoflowers, a SADI experiment was performed. Nitrogen-adsorption isotherms of the PtNi-H/MWCNT nanoflowers (Fig. 2) exhibit a steep increase in the curve at a relative pressure of  $0.9 < P/P_0 < 1.0$ , which is assigned to the presence of mesoporous structures [27]. The profile of the hysteresis loop at  $P/P_0$  between 0.8 and 1.0 (the insert in Fig. 2A) is also an adsorption-desorption characteristics of porous materials. Correspondingly, the dominating distribution of pore sizes was 3.0–8.0 nm (Fig. 2B) calculated by the Barrett–Joyner–Halenda method. The Brunauer–Emmett–Teller (BET) surface area of the PtNi-H/MWCNT nanoflowers is measured to be 63.58 m<sup>2</sup> g<sup>-1</sup>, which is 5 times larger than the value of 12.50 m<sup>2</sup> g<sup>-1</sup> calculated for the surface of dense spheres. Obviously, the porous PtNi-H/MWCNT nanoflowers can be expected to achieve higher catalytic performance and utilization efficiency of PtNi alloy catalysts due to the relatively lower density and higher surface area.

Fig. 3 shows the XRD patterns of the PtNi-H/MWCNT nanoflowers and commercial Pt/C-JM, in which the characteristic peaks from a crystalline face centered cubic (fcc) Pt phase appear at the corresponding diffraction angles for the (111), (200), (220), and (311) fundamental peaks. The typical fcc-Pt diffraction peaks in the PtNi-H/MWCNT nanoflowers seem to be broadened and there are no noticeable peaks for phase separated structures such as a pure Ni or its oxides in XRD measurements, indicating a good degree of alloying between Pt and Ni. In particular, the diffraction peaks were slightly shifted to the high  $2\theta$  values in the PtNi particles as

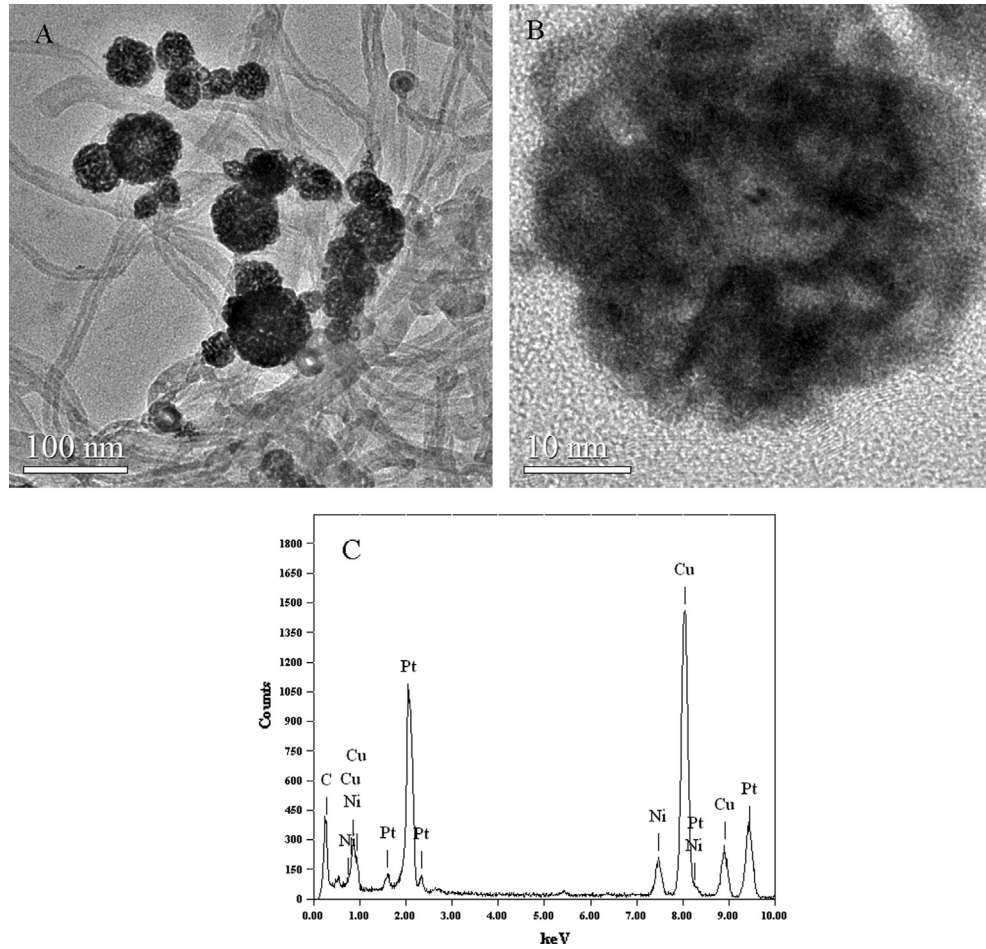


**Fig. 1.** Morphological and structural characterizations of the PtNi-H/MWCNT nanoflowers: (A) low resolution TEM; (B) magnified TEM. (C) EDS spectrum of the PtNi-H/MWCNT nanoflowers.

compared to those of the pure Pt particles, in agreement with Vegard's law [28,29].

### 3.3. Electrochemical properties of PtNi-H/MWCNT nanoflowers

According to a previous report, Pt{111} shows higher ORR activity in a perchloric acid than sulfuric acid because sulfate ions are adsorbed on the Pt{111} surface more strongly [30]. Thus, to investigate the electrocatalytic activity of the {111}-enclosed PtNi—

H/MWCNT nanoflowers for the ORR, we have performed electrochemical experiments in  $N_2$ -saturated 0.1 M  $HClO_4$  solution. Fig. 4A shows CVs of the PtNi-H/MWCNT nanoflowers and commercial Pt/C-JM. As observed, a relatively intense peak at 0.1 V compared to the peak in the 0.20–0.30 V range indicate that the PtNi-H/MWCNT nanoflowers mainly consist of Pt{111} facets [31–33]. In the cathodic scan, the reduction peak potential of the Pt oxide for the PtNi-H/MWCNT nanoflowers has 26 mV positive shifts compared to commercial Pt/C-JM, indicating weaker binding of the oxygenated

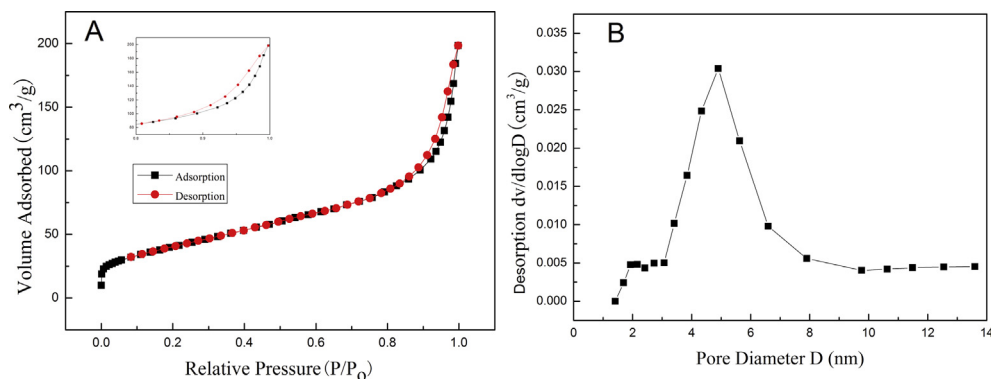


**Fig. 2.** (A) Typical nitrogen adsorption–desorption isotherm of the PtNi-H/MWCNT nanoflowers and (B) the corresponding pore-size distribution curve obtained from the Barrett–Joyner–Halenda method. The insert in (A) shows the magnified hysteresis loop at  $P/P_0$  between 0.8 and 1.0.

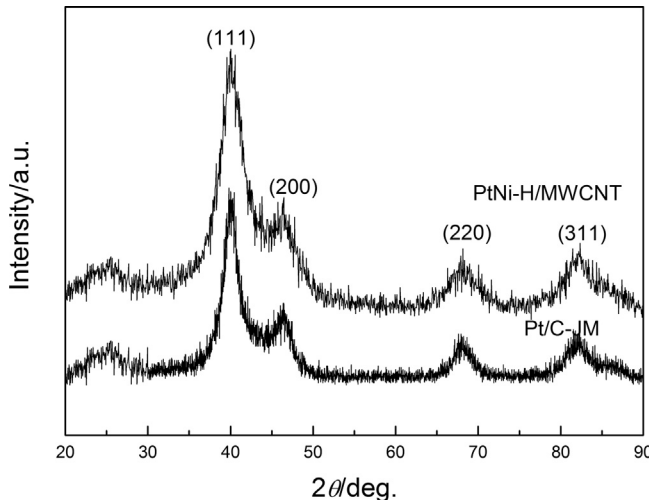


**Fig. 3.** XRD patterns of the PtNi-H/MWCNT nanoflowers and commercial Pt/C-JM.

species on the surface of the PtNi-H/MWCNT nanoflowers. The weak oxophilicity will be a benefit for enhancing electrocatalytic activity for ORR. Fig. 4B shows the polarization curves of the PtNi-H/MWCNT nanoflowers and commercial Pt/C-JM. From 0.70 to 1.0 V is the mixed kinetic-diffusion controlled region, and the ORR goes

continuously to the diffusion-limiting current region when the potential is more negative than 0.70 V. Clearly, the PtNi-H/MWCNT nanoflowers exhibit a more positive onset potential and higher activity than commercial Pt/C-JM. In addition, the PtNi-H/MWCNT nanoflowers exhibit a higher ORR current in the mixed kinetic-diffusion controlled region than commercial Pt/C-JM, supporting its superior ORR activity. The electrochemically active surface area (ECSA) specific current density ( $i_k$ ) represents the intrinsic activity of catalysts, which is a better indicator of an electrocatalysts' quality. To further compare the ORR activity, ECSA specific kinetic activities were shown in Fig. 4C. The PtNi-H/MWCNT nanoflowers show greater ECSA specific kinetic activity than the commercial Pt/C-JM in the whole potential range (0.85–0.95 V). For example, as shown Fig. 4D, the specific kinetic current density is  $4.41 \text{ mA cm}^{-2}$  for the PtNi-H/MWCNT nanoflowers at 0.80 V which is 1.24 times of that for the commercial Pt/C-JM ( $3.57 \text{ mA cm}^{-2}$ ). These results indicate that the PtNi-H/MWCNT nanoflowers have higher electrocatalytic activity for the ORR than the commercial Pt/C-JM at the same Pt loading.

Recently, the durability of electrocatalytic materials has been recognized as one of the most important issues before the commercial application of fuel cells [34,35]. Herein, the accelerated durability test of the ORR was carried out by applying linear potential sweeps between 0.2 and 1.0 V for 800 cycles with a scan rate of  $50 \text{ mV s}^{-1}$  in  $\text{O}_2$ -saturated 0.1 M  $\text{HClO}_4$  solution. After 800 cycles, a 10 mV negative-shift at the half-wave potential is observed for the

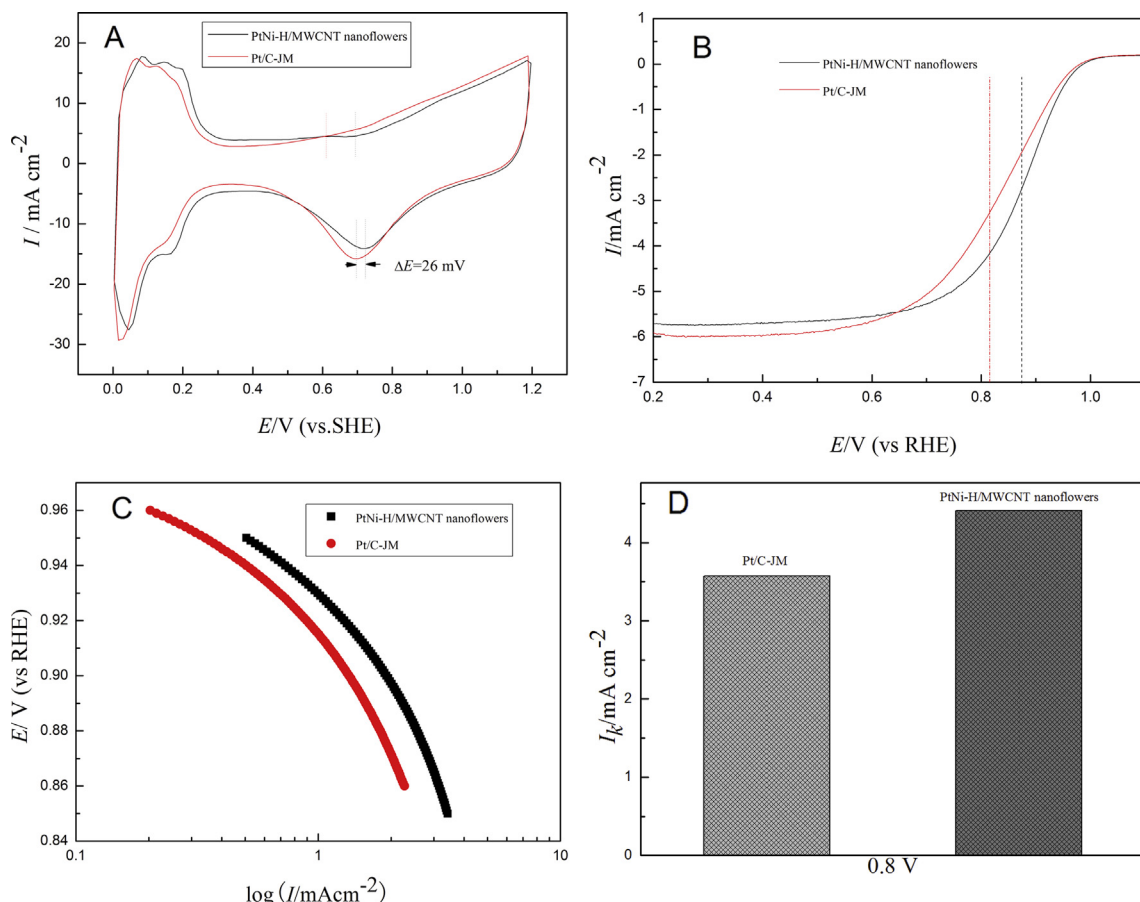


**Fig. 4.** (A) CV curves for the PtNi-H/MWCNT nanoflowers and commercial Pt/C-JM in  $\text{N}_2$ -saturated  $0.1 \text{ mol L}^{-1} \text{ HClO}_4$  solution at a scan rate of  $50 \text{ mV s}^{-1}$ . (B) ORR polarization curves for the PtNi-H/MWCNT nanoflowers and commercial Pt/C-JM in  $\text{O}_2$ -saturated  $0.1 \text{ mol L}^{-1} \text{ HClO}_4$  solution at a scan rate of  $5 \text{ mV s}^{-1}$  and rotation rate of  $1600 \text{ rpm}$ . (C) Specific kinetic current densities ( $i_k$ ) for the PtNi-H/MWCNT nanoflowers and commercial Pt/C-JM at different potentials. (D) Specific kinetic current densities for the PtNi-H/MWCNT nanoflowers and commercial Pt/C-JM at  $0.80 \text{ V}$ .

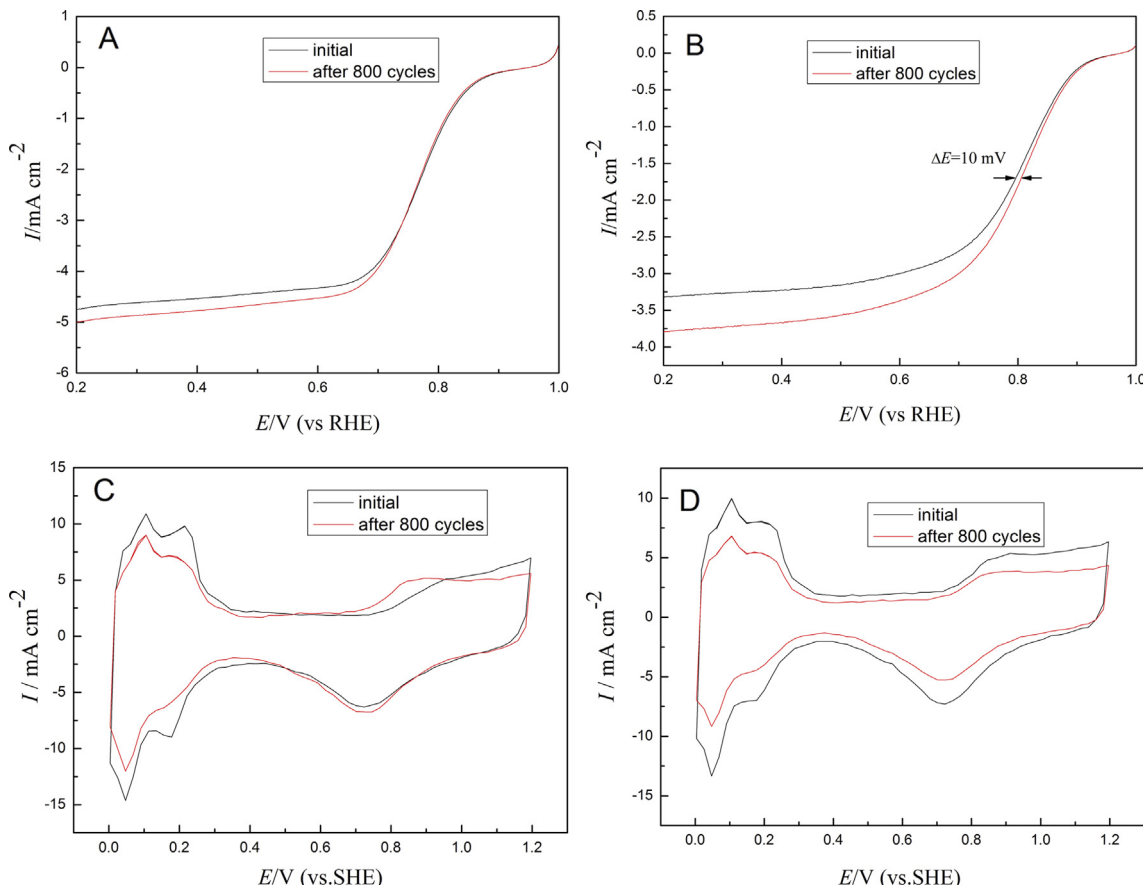


**Fig. 5.** ORR polarization curves for (A) the PtNi-H/MWCNT nanoflowers and (B) commercial Pt/C-JM in O<sub>2</sub>-saturated 0.1 M HClO<sub>4</sub> solution before and after 800 potential cycles at a scan rate of 5 mV s<sup>-1</sup> and rotation rate of 1600 rpm; CV curves for (C) the PtNi-H/MWCNT nanoflowers and (D) commercial Pt/C-JM in O<sub>2</sub>-saturated 0.1 M HClO<sub>4</sub> solution before and after 800 cycles at a scan rate of 50 mV s<sup>-1</sup>.

commercial Pt/C-JM (Fig. 5B), while there is almost no negative-shift for the PtNi-H/MWCNT nanoflowers (Fig. 5A). This is direct evidence that the PtNi-H/MWCNT nanoflowers have better stability for the ORR compared to commercial Pt/C-JM. The loss of stability of Pt catalysts generally stems from the aggregation of the Pt nanoparticles themselves because of Ostwald ripening [36,37]. Therefore, the ECSA of the PtNi-H/MWCNT nanoflowers and commercial Pt/C-JM before and after the durability tests were also measured. As shown in Fig. 5C, D, the PtNi-H/MWCNT nanoflowers exhibit a negligible loss of 10.08% in ECSA after durability test, whereas commercial Pt/C-JM exhibit an obvious loss of 32.35%. The ECSA of catalysts were calculated from integrated hydrogen adsorption/desorption region (0–0.4 V vs SHE) of the CV curves using 0.21 mC cm<sup>2</sup> Pt as the conversion factor.

#### 4. Conclusion

In summary, we reported a simple and straightforward route to synthesize the porous PtNi-H/MWCNT alloy nanoflowers with high shape selectivity via a novel and potentially general one-pot reaction that exploits an in situ sacrificial template. The obtained PtNi-H/MWCNT alloy nanoflowers exhibited superior ORR activity and long-term durability compared to commercial Pt/C-JM due to the change of the binding energy of Pt (i.e., electronic effect), decrease in Pt–Pt bond length (geometric effect). Thus, the superior performance of the PtNi-H/MWCNT alloy nanoflowers made it a promising cathode electrocatalyst in DAFCs.

#### Acknowledgments

This project was supported by the National Undergraduate Training Programs for Innovation and Entrepreneurship (201310446016), the Excellent Middle-age and Young Scientists Research Award Foundation of Shandong Province (BS2010NJ008) and the Shandong Province Postdoctoral Innovation Foundation Funded Project (No. 201203042).

#### References

- [1] S. Zhang, X.Z. Yuan, J.N.C. Hin, H. Wang, K.A. Friedrich, M. Schuze, *J. Power Sources* 194 (2009) 588–600.
- [2] C. Wang, H. Daimon, T. Onodera, T. Koda, S.H. Sun, *Angew. Chem.* 47 (2008) 3588–3591.
- [3] R.J. Jafri, N. Sujatha, N. Rajalakshmi, S. Ramaprabhu, *Int. J. Hydrogen Energy* 34 (2009) 6371–6376.
- [4] N.M. Markovic, T.J. Schmidt, V. Stamenovic, P.N. Ross, *Fuel Cells* 1 (2001) 105–116.
- [5] Y. Bing, H. Liu, L. Zhang, D. Ghosh, J. Zhang, *Chem. Soc. Rev.* 39 (2010) 2184–2202.
- [6] Y. Chen, F. Yang, Y. Dai, W. Wang, S. Chen, *J. Phys. Chem. C* 112 (2008) 1645–1649.
- [7] Y. Xing, Y. Cai, M.B. Vukmirovic, W.P. Zhou, H. Karan, J.X. Wang, et al., *J. Phys. Chem. Lett.* 1 (2010) 3238–3242.
- [8] A. Seo, J. Lee, K. Han, H. Kim, *Electrochim. Acta* 52 (2006) 1603–1611.
- [9] E. Antolini, J.R.C. Salgado, M.J. Giz, E.R. Gonzalez, *Int. J. Hydrogen Energy* 30 (2005) 1213–1220.
- [10] Y.H. Cho, T.Y. Jeon, J.W. Lim, Y.H. Cho, M. Ahn, N. Jung, et al., *Int. J. Hydrogen Energy* 36 (2011) 4394–4399.
- [11] C.S. Rao, D.M. Singh, R. Sekhar, J. Rangarajan, *Int. J. Hydrogen Energy* 36 (2011) 14805–14814.
- [12] M.A. Garcia-Contreras, S.M. Fernandez-Valverde, J.R. Vargas-Garcia, M.A. Cortes-Jacome, J.A. Toledo-Antonio, C. Angeles-Chavez, *Int. J. Hydrogen Energy* 33 (2008) 6672–6680.

- [13] F. Kadirgan, A.M. Kannan, T. Atilan, S. Beyhan, S.S. Ozenler, S. Suzer, et al., Int. J. Hydrogen Energy 34 (2009) 9450–9460.
- [14] E.B. Fox, H.R. Colon-Mercado, Int. J. Hydrogen Energy 35 (2010) 3280–3286.
- [15] T. Toda, H. Igarashi, M. Watanabe, J. Electroanal. Chem. 460 (1999) 258–262.
- [16] H. Yang, C. Coutanceau, J.-M. Leger, N. Alonso-Vante, C. Lamy, J. Electroanal. Chem. 576 (2005) 305–313.
- [17] R.C. Koffi, C. Coutanceau, E. Garnier, J.-M. Leger, C. Lamy, Electrochim. Acta 50 (2005) 4117–4127.
- [18] V. Baglio, A.S. Arico, A. Stassi, C. D'Urso, A.D. Blasi, A.M. Castroluna, et al., J. Power Sources 159 (2006) 900–904.
- [19] A. Stassi, C. D'Urso, V. Baglio, A.D. Blasi, V. Antonucci, A.S. Arico, et al., J. Appl. Electrochem. 36 (2006) 1143–1149.
- [20] V. Baglio, A. Stassi, A.D. Blasi, C. D'Urso, V. Antonucci, A.S. Arico, Electrochim. Acta 53 (2007) 1360–1364.
- [21] X. Teng, X. Liang, S. Maksimuk, H. Yang, Small 2 (2005) 249–253.
- [22] Z. Yang, Y. Lu, Chem. Commun. (2009) 2270–2277.
- [23] J.H. Shim, Y.S. Kim, M. Kang, C. Lee, Y. Lee, Phys. Chem. Chem. Phys. 14 (2012) 3974–3979.
- [24] I. Pastoriza-Santos, L.M. Liz-Marzan, Langmuir 18 (2002) 2888–2894.
- [25] H.S. Shin, H.J. Yang, S.B. Kim, M.S. Lee, J. Colloid Interface Sci. 274 (2004) 89–94.
- [26] Y. Vasquez, A.K. Sra, R.E. Schaak, J. Am. Chem. Soc. 127 (2005) 12504–12505.
- [27] Z. Sun, L. Wang, P. Liu, S. Wang, B. Sun, D. Jiang, F.S. Xiao, Adv. Mater. 18 (2006) 1968–1971.
- [28] A.R. Denton, N.W. Ashcroft, V. Law, Phys. Rev. A 43 (1991) 3161–3164.
- [29] K. Ahrenstorff, O. Albrecht, H. Heller, A. Kornowski, D. Golitz, H. Weller, Small 3 (2007) 271–274.
- [30] C.M. Sanchez-Sanchez, J. Solla-Gullon, F.J. Vidal-Iglesias, A. Aldaz, V. Montiel, E. Herrero, J. Am. Chem. Soc. 132 (2010) 5622–5624.
- [31] M.N. Mankin, V. Mazumder, S. Sun, Chem. Mater. 23 (2010) 132–136.
- [32] R. Loukrakpam, P. Chang, J. Luo, B. Fang, D. Mott, I.T. Bae, H.R. Naslund, M.H. Engelhard, C.J. Zhong, Chem. Commun. 46 (2010) 7184–7186.
- [33] F.J. Vidal-Iglesias, R.M. Aran-Ais, J. Solla-Gullon, E. Herrero, J.M. Feliu, ACS Catal. 2 (2012) 901–910.
- [34] H.W. Liang, X.A. Cao, F. Zhou, C.H. Cui, W.J. Zhang, S.H. Yu, Adv. Mater. 23 (2011) 1467–1471.
- [35] K. Sasaki, H. Naohara, Y. Cai, Y.M. Choi, P. Liu, M.B. Vukmirovic, J.X. Wang, R.R. Adzic, Angew. Chem. Int. Ed. 49 (2010) 8602–8607.
- [36] I.E.L. Stephens, A.S. Bondarenko, U. Gronberg, J. Rossmeisl, I. Chorkendorff, Energy Environ. Sci. 5 (2012) 6744–6762.
- [37] K. Hartl, M. Hanzlik, M. Arenz, Energy Environ. Sci. 4 (2010) 234–238.